Bulletin of Electrical Engineering and Informatics
Vol. 15, No. 6, December 2026, pp. 5079~5091
ISSN: 2302-9285, DOI: 10.11591/eei.v15i6.14184

Adaptive multi-domain framework for noise classification and image denoising

Shilpa Hiremath[1,2], A. Shobha Rani[1,2]
[1]Department of Electronics and Communication Engineering, BMS Institute of Technology & Management, Bangalore, India
[2]Visvesvaraya Technological University, Belagavi, Karnataka, India

Article Info

Article history:

Received Aug 7, 2026
Revised Sep 18, 2026
Accepted Oct 4, 2026

Keywords:

Curvature penalty
Dempster–Shafer fusion
Entropy-guided rank-order filtering
Image denoising
Monogenic signal analysis
Noise classification
Riemannian manifold diffusion

ABSTRACT

The real-world imaging systems is the most challenging task, as the images suffer from various types of noise that occur during acquisition or transmission. As the cause for each noise is different, their characteristics are also different. Hence, there arise the need for a method which can denoise the image irrespective of its characteristic and manage the image. To address this challenge, this study presents a three-stage image enhancement structure. First is the identification of the noise in an image, then based on the characteristic of the noise three different filters are applied parallelly to supress each characteristic. The output obtained from each filtered result is fused at pixel level through a reliability-based fusion strategy. The proposed work considers various concepts i.e., mathematical concepts, rank order guided by entropy, and the curvature constraints with variational optimization. In fusion method, decision mechanism based on the evidence is used as it provides a reliable image feature. The proposed technique is proved by considering 5 different noise models and the experimental outcomes confirmed at a noise level of sigma=25 with an average peak signal-to-noise ratio (PSNR) of 39.84 dB and a structural similarity index measure (SSIM) of 0.974. Also, the method consistently achieved improvements of approximately 3.2–3.7 dB.

This is an open access article under the CC BY-SA license.

Corresponding Author:

Shilpa Hiremath
Department of Electronics and Communication Engineering, BMS Institute of Technology & Management
Bangalore 560064, India
Email: shilpasharankh@bmsit.in

1. INTRODUCTION

Digital imaging plays an important role in modern electrical, electronic, and informatics systems, including charge-coupled device (CCD)/complementary metal-oxide-semiconductor (CMOS) imaging sensors, surveillance platforms, industrial inspection systems, medical imaging devices, remote sensing, and embedded vision applications. In such systems, acquired images are frequently used for monitoring, detection, recognition, measurement, and automated decision-making. Noise introduced during image acquisition, sensing, transmission, and electronic processing can degrade image quality and adversely affect subsequent visual analysis and information-processing tasks [1]-[4]. Recent studies have further emphasized that denoising remains an important component of imaging pipelines because the quality of restored images can influence feature extraction, segmentation, recognition, and other downstream operations [2], [3], [5]. Image degradation may arise from sensor imperfections, thermal and electronic fluctuations, photon-limited acquisition, transmission disturbances, and application-specific imaging mechanisms [1], [4], [6]. Therefore, effective noise characterization and restoration are important not only for improving visual image quality but also for supporting reliable operation of practical electronic imaging and intelligent vision systems.

Image denoising is challenging because different noise types exhibit different statistical and structural characteristics. Gaussian noise is commonly associated with electronic and thermal disturbances, impulse noise may result from transmission errors, Poisson noise is associated with photon-limited acquisition, while speckle and other structured noise can arise in specific imaging modalities [7]. A restoration method that performs effectively for one degradation model may not provide comparable performance for another. Furthermore, excessive filtering can remove important edges, textures, and fine image details, whereas insufficient filtering may leave residual noise that affects subsequent processing. Recent reviews have identified the balance between noise suppression and detail preservation, together with robustness to unknown noise characteristics and generalization to practical imaging conditions, as continuing challenges in image denoising [8]. Consequently, the use of a single fixed denoising mechanism may be insufficient when noise characteristics vary across different imaging conditions.

Recent research has investigated conventional, adaptive, deep learning-based, blind, and self-supervised approaches to address these challenges. Comprehensive recent reviews have documented the evolution from classical model-based techniques toward convolutional neural networks, transformers, self-supervised learning, and other modern restoration strategies [9]. Practical blind denoising methods have been developed to address unknown and complex degradation conditions, while dynamic and adaptive neural architectures have attempted to improve restoration under varying noise levels [10]-[13]. Self-supervised approaches have also attracted increasing attention because they can reduce dependence on paired noisy-clean training data [14]-[17]. In addition, lightweight and efficient transformer-based models have been proposed to address the computational requirements associated with practical image restoration [5], [13]. Adaptive and hybrid filtering strategies continue to demonstrate the importance of adjusting restoration according to image and noise characteristics [18]. These studies have substantially advanced denoising performance; however, many approaches are designed around a particular network architecture, training strategy, or restoration mechanism, and their effectiveness may depend on assumptions regarding training data, noise distributions, computational resources, or degradation conditions.

Based on these observations, a research gap exists in the explicit integration of noise characterization, noise classification, complementary restoration mechanisms, and reliability-based fusion within a unified and interpretable framework. Existing blind and self-supervised approaches primarily focus on learning a direct restoration mapping under unknown noise conditions [10], [14]-[17], whereas adaptive neural approaches generally modify network behavior or restoration parameters through learned representations [11]-[13]. Similarly, recent adaptive filtering methods improve restoration by tuning or combining particular filtering operations [18]. However, there remains scope for a structured framework that explicitly analyzes noise characteristics before restoration, uses complementary spatial and spectral information for noise characterization, classifies the dominant degradation, and subsequently integrates multiple deterministic restoration outputs according to their reliability. These limitations motivate the development of an adaptive framework that explicitly connects noise identification and classification with the subsequent restoration process.

To address this problem, this study proposes an adaptive multi-domain framework for noise classification and image denoising. The proposed framework analyzes degraded images using complementary spatial and spectral characteristics to identify the dominant noise category. A random forest classifier is employed for noise classification and confidence estimation. Subsequently, three complementary deterministic restoration mechanisms, namely Riemannian manifold diffusion, entropy-guided rank-order filtering, and curvature-constrained variational filtering, are applied in parallel. The resulting restoration outputs are integrated using a reliability-based fusion mechanism based on local image characteristics and classification information. By separating noise characterization from restoration, the framework aims to adapt the restoration process to the observed degradation characteristics rather than relying on a single fixed denoising strategy.

The new value of this work lies in the structured integration of multi-domain noise characterization, explicit noise classification, complementary deterministic filtering, and reliability-based image fusion within a unified adaptive restoration framework. Unlike approaches that depend exclusively on a single filtering technique or an end-to-end learning model, the proposed framework combines spatial and spectral information with a random forest-based noise classifier and multiple restoration branches to exploit complementary denoising characteristics. The principal innovation is therefore the explicit connection between noise identification and restoration through a multi-stage adaptive processing pipeline. This design is relevant to intelligent electronic imaging and vision-based information-processing systems in which variations in noise characteristics can affect image quality and the reliability of subsequent processing tasks.

2. PROPOSED SYSTEM ARCHITECTURE

The proposed method is a three-stage process that helps improve image quality. It finds the type of noise in the image and uses the right techniques to fix it. The system takes an image of any size as input and

produces a restored image of the same size with good quality. To handle colour images better the input image is changed from red, green, and blue (RGB) to YC_bC_r format [19], [20]. The main part of the image (Y) which has most of the information goes through the whole restoration process. The other parts (C_b and C_r) which have visual information are processed using a simpler filtering method. After restoration the three parts are combined to create the output image. The proposed work has three phases.

- The first phase identifies the noise in the image and how much it degrades the image.
- The second phase applies three filtering techniques at the same time. Each technique targets a type of noise.
- The last phase combines the filtered results into an image with accurate restoration.

A final step enhances image sharpness. The restored image is then converted back to its RGB color representation. This multi-stage design helps the system adapt to noise conditions. It also preserves image details and produces a restored image with high quality. The restored image has the dimensions and bit depth, as the input image. Figure 1 shows the working process of the proposed system. Table 1 shows the function of each block considered in the proposed diagram, along with the input provided to each block and the result obtained from each block.

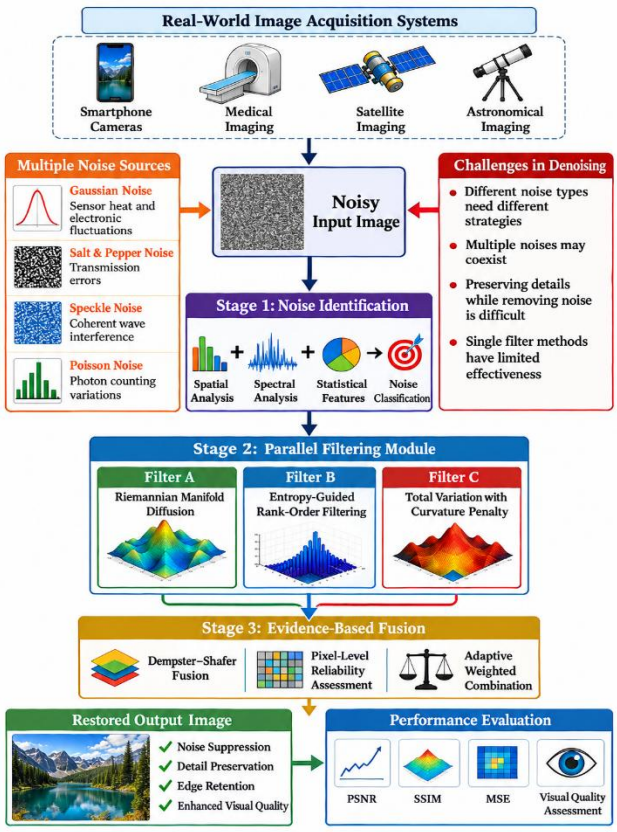


Figure 1. Overview of the proposed framework

Table 1. Blocks of proposed diagram showing their input, output and their function

Stage	Block	Input	Output	Core function
0	Noisy image input	Raw pixel data from sensor or file	Pixel matrix passed inward	Entry point; standardises bit-depth and colour space.
1	Noise identification	Standardised pixel matrix	Noise class+ severity estimate	Characterises noise statistically; outputs class label λ and $\hat{\sigma}$.
2a	Filter 1	Pixel matrix+ $\{\lambda, \hat{\sigma}\}$	Image F_1	Geometry aware manifold diffusion along image structure.
2b	Filter 2	Pixel matrix+ $\{\lambda, \hat{\sigma}\}$	Image F_2	Local entropy driven rank order pixel selection.
2c	Filter 3	Pixel matrix+ $\{\lambda, \hat{\sigma}\}$	Image F_3	Variational energy minimisation with curvature constraint.
3	Image fusion	F_1, F_2, F_3+ noise posteriors	Single best estimate image $\hat{I}$	Evidence theoretic pixel-level fusion using phase coherence.
4	Noise-free output image	Fused image $\hat{I}$	Restored image delivered to user	Final sharpening and colour-space reconversion.

3. NOISE IDENTIFICATION MODULE

The combination of both spectral and spatial features to accurately classify the dominant noise present in an input image is the proposed noise identification block. With the help of two-dimensional discrete Fourier transform (2D-DFT) the image is first converted to frequency domain, the Renyi entropy values are helping to distinguish between noise categories, like Gaussian noise and periodic noise and Speckle noise. The Renyi entropy is given by:

$$H(a) = \frac{1}{1-a}.log_2 \sum_{u,v} P(u,v)^a \text{ for } \alpha \neq 1 \text{ where } P(u,v) = \frac{|F(u,v)|^2}{\sum_{u,v}|F(u,v)|^2}$$

The spectral features give us information that is based on frequency. The spatial features tell the relation between pixels that are next to each other. To get these characteristics we capture the image then by subtracting a version of the image that has been smoothed a little from the image. This residual image shows the noise components clearly but it does not show the big structures in the image. Moran's Autocorrelation Index is used to measure how the pixels in the image are related to each other. This measure tells if the pixels that are next to each other have random or opposite patterns. If the values are positive, it means the pixels are clustered together which is often the case with speckle or periodic noise. If the values are close to zero it means the noise is random. If the values are really negative it often means image is dealing with noise patterns. This information helps to understand the analysis better and makes the classification more reliable. The spatial features and the spectral features work together to give an understanding of the image. The Moran's Autocorrelation Index is a tool for analyzing the spatial behavior of the residual image. The residual image is a part of this process because it helps to perceive the noise components clearly. The spectral features and the spatial features are both important, for classification.

$$R(x,y) = I(x,y) - [G\sigma\ = 1.0\ \otimes\ I](x,y) \text{ where } I(M) = \frac{M}{W}.\frac{\sum_i \sum_j w_{i,j}(R_i-\bar{R})(R_j-\bar{R})}{\sum_i (R_i-\bar{R})^2}$$

3.1. Noise classification

The features from the image both spectral and spatial are combined to create one feature vector. This vector describes the image characteristics. The feature vector is then given to a random forest classifier [21]. This classifier has one hundred decision trees. The classifier is trained with artificially degraded images. These images include types of noise and various noise levels. Tests during the study showed that the classifier can accurately identify six noise categories. It also determines the likely noise type. The classifier generates probability values for all classes. These values show how confident the prediction is. They are used later in the image fusion process. The classification stage provides the predicted noise class and its confidence score. This helps the framework make image restoration decisions. The classifiers output is useful for image restoration. It provides a way to measure the confidence, in the predicted noise class.

Algorithm 1. Noise identification and classification
Input: Noisy image (I)
Output: Predicted noise class (**λ**) and estimated noise level (**$\hat{\sigma}$**)

1. Convert the input RGB noisy image (I) into the YCbCr color space.
2. Extract the luminance component (Y).
3. Calculate the two-dimensional discrete Fourier transform of (Y) to obtain (F(u,v)).
4. Compute the normalized power spectrum: $P(u,v)=|Fu,v)|^2/\sum_{u,v}|Fu,v)|^2$
5. Estimate the Rényi entropy of order two: $H2 =-\log(\sum_{u,v} P(u,v)^2)$
6. Generate the residual image (R).
7. Find the mean residual value: $\bar{R}=(1/n)\sum_i R_i$
8. Calculate Moran's spatial autocorrelation: $I_m=(n/W)\times[\sum_i\sum_j w_{ij}(R_i-\bar{R})(R_j-\bar{R})]/[\sum_i(R_i-\bar{R})^2]$
9. Construct the two-dimensional feature vector: $F=[H_2,I_m]$
10. Normalize the feature vector to obtain (F_{norm}).
11. Apply the 100-tree Random Forest classifier: $\lambda=RF_{100}(F_{norm})$
12. Estimate the noise level using Haar-wavelet MAD: $\hat{\sigma}=\text{median}(|d_i|)/0.6745$
13. Return the predicted noise class λ and estimated noise level $\hat{\sigma}$

The feature ranges presented in Table 2 were obtained from the observed distributions of the extracted Moran's autocorrelation index and Rényi entropy values for the artificially degraded training images representing the considered noise categories. These ranges were used to summarize the characteristic feature

behavior of the respective noise classes and to provide an interpretable representation of the relationship between the noise characteristics and the corresponding restoration strategy.

Table 2. Various noise classes there feature ranges, filter assignments, and threshold parameters

Class	Physical origin	Moran I_M	Renyi H_2	Lead filter	α_λ weight
Gaussian [22]	Thermal sensor fluctuation	−0.02–0.04	6.8–7.4	Filter 1	0.80
Salt-pepper [23]	Transmission bit errors	−0.91–−0.80	5.1–5.9	Filter 2	2.00
Speckle [24]	Coherent illumination scatter	0.18–0.35	6.2–6.7	Filter 3	1.20
Poisson [25]	Low-photon-count imaging	0.01–0.09	6.5–7.1	Filter 1	1.00
Periodic [26]	Power-line/scan banding	0.60–0.90	3.8–4.6	Filter 3	1.60
Mixed (Gaussian and salt and pepper)	Combined thermal+digital	−0.40–−0.10	5.8–6.4	Filters 1+2	1.40

Importantly, the numerical ranges in Table 2 are not used as hard decision thresholds for the final noise classification. The actual noise identification is performed by the 100-tree random forest classifier using the extracted feature vector and its learned decision structure. Therefore, small variations in the tabulated range boundaries do not directly alter the classifier decision, since classification is not based on manually defined threshold comparisons.

The lead-filter assignments summarize the restoration strategy associated with the predicted dominant noise category, while the corresponding αλ values represent class-dependent parameters used in the adaptive filtering process. These assignments were selected according to the complementary characteristics of the three restoration mechanisms and their suitability for the corresponding noise conditions considered in the experimental framework.

4. FILTERING STRATEGY

The research framework uses three filtering methods namely:

Filter 1: Riemannian manifold diffusion where the image is represented as a geometric surface in which pixel intensity defines the surface height. This method avoids the edge detection method as it enables adaptive diffusion which smoothens the homogeneous regions also preserving the boundaries of the object. The geometric metric and conductance function are given by:

$$g(x,y) = I_2 + \rho(\nabla I(x,y) \otimes \nabla I(x,y))$$

$$c(x,y) = 1/(\, exp((|\nabla I|^2 - EF)/Teff) + 1)$$

The restored image is found by iterative manifold diffusion given by:

$$\partial u/\partial t = c(x,y)\Delta_g\, u$$

$$\Delta_g u = (1/\sqrt{det(g)})\, \partial_i(\sqrt{det(g)}\, g^{ij}\, \partial_j u)$$

where Δ_g represents the Laplace–Beltrami operator.

Filter 2: entropy-guided rank-order filter where the strategy is to compute local Shannon entropy to distinguish between smooth and textured areas. Below equations shows the filtering rank is adaptively selected based on the local complexity, allowing effective impulse noise removal while preserving image details. An adaptive threshold, further improves suppression of highly corrupted pixels.

$$r(x,y) = r_{min} + (r_{max} - r_{min})\sigma[\beta(H{\sim}(x,y) - 0.5)]$$

$\tau = \tau_{base} + \alpha_\lambda, \hat{\sigma}$, where $\tau_base = 0.03$

Filter 3: curvature constrained variational filter-the restored image is estimated by minimizing an energy function that jointly preserves image fidelity, smoothness, and structural continuity, this framework incorporates curvature information to accurately preserve object boundaries and curved structures.

$$E[u] = (\lambda/2)\|u - I\|^2{}_\Omega + \alpha TV(u) + \beta C(u)$$

$$\kappa(u) = (u_{xx}{u_y}^2 - 2u_{xy}u_x u_y + u_{yy}{u_x}^2)/({u_x}^2 + {u_y}^2)^{3/2}$$

5. IMAGE FUSION MODULE

The system has three ways to restore the images once the three-stage filtering is completed. Rather than considering the single filtered output, Dempster–Shafer image fusion combines the output of all the three filters characteristic to produce the more reliable restoration outcome. The fusion module ensures to consider the valid information at every pixel and neglect the weak information from the three filter results to achieve the good quality image. The fusion weight distribution across various regions in an image is mentioned in Table 3.

The local structural characteristics of an image namely: amplitude, phase, and orientation are analysed and the quality of each restored image is evaluated. This helps to considerate the hidden information provided by every filtered result. Structural comparison of the noisy image with the restored image helps in proper framing of the model and also ensures the effective result produced by the filtering techniques. The system measures how consistent the structure is and turns this into reliability scores. These scores show how confident images are in each filters output. The scores consider two things:

- The characteristics of the image locally.
- The information about the noise that was classified during the processing stage.

This helps the system choose filters that are a good match, for the type of noise detected. The filters that are really reliable have larger influence while the ones that are not as reliable are with lesser weights. This means that the final picture is made by combining the weights of each filter output. The system looks at each pixel separately and combines the filter outputs in a way that adapts to each pixel location based on local image conditions. Different parts of the image can be made from different combinations of filter outputs because each part of the picture is unique and may have been degraded in different ways. The reliability scores of the filters are what make this possible by helping the system figure out which filter outputs to consider more.

Table 3. Typical fusion weight distribution W_1, W_2, W_3 by region type, and averaged over the test set

Region type	W_1 (filter 1)	W_2 (filter 2)	W_3 (filter 3)	Reason for distribution
Flat homogeneous area	0.28	0.16	0.56	Variational filter produces cleanest flats; little edge to protect.
Strong edge pixel	0.58	0.09	0.33	Manifold diffusion best follows geometry without crossing boundaries.
Rich texture zone	0.22	0.58	0.20	Rank-order selection preserves local intensity histogram distribution.
Impulse-hit pixel	0.08	0.83	0.09	Only rank-order filtering reliably eliminates extreme outlier values.
Curved boundary	0.38	0.14	0.48	Curvature penalty in Filter 3 keeps contours smooth and natural.

6. EXPERIMENTAL RESULTS

6.1. Setup

All tests ran on a workstation with an AMD Ryzen 9 7950X 128 GB RAM and 16-core processor. No GPU was used at any stage. The system was implemented in Python 3.11, relying on NumPy and SciPy for numerical operations and scikit-learn for the random forest classifier. Competing methods were evaluated using their authors' published implementations with their recommended default parameters; none were re-tuned for this comparison. Five benchmark datasets were used. Table 4 describes each dataset which covers different image content and noise models, providing a diverse evaluation across realistic imaging scenarios.

Table 4. Benchmark datasets

Dataset	Count	Resolution	Scene type	Noise added	Evaluation purpose
BSD68	68	481×321	Natural photographs	Gaussian, $\sigma \in \{10,25,50,75\}$	Primary denoising benchmark
Set12	12	256×256	Standard test images	Gaussian, $\sigma \in \{15,25,50\}$	Classic single-image tests
Urban100	100	Varied	Buildings, roads, and grids	All six noise types	Structural integrity testing
CBSD68	68	481×321	Colour photographs	Gaussian+Speckle	Colour fidelity evaluation
MedNoise-50	50	512×512	MRI and CT slices	Rician+Poisson	Clinical imaging validation

Table 5 summarizes the color-image processing strategy used in the proposed framework. The conversion to the YCbCr representation enables the primary adaptive restoration process to focus on the luminance component, which contains the dominant structural and intensity information, while the chrominance components are processed separately and incorporated during color-image reconstruction. The CBSD68 dataset is included to evaluate the framework on color photographs under Gaussian and speckle noise

conditions. The quality of the reconstructed output is assessed using the overall image-quality measures peak signal-to-noise ratio (PSNR), structural similarity index measure (SSIM), mean squared error (MSE), feature similarity index measure (FSIM), and learned perceptual image patch similarity (LPIPS) together with visual inspection. A dedicated chrominance-specific color-difference analysis is not included in the present study; therefore, the results should be interpreted as an evaluation of overall reconstructed-image quality.

Table 5. Color-image processing strategy and evaluation coverage in the proposed framework

Processing stage	Color component	Processing strategy	Purpose	Evaluation evidence
Color-space conversion	RGB→YCbCr	Input color images are transformed into YCbCr representation.	Separates luminance information from chrominance information.	Color-image processing framework.
Primary restoration	Y (luminance)	Complete proposed adaptive noise identification, parallel filtering, and fusion framework.	Restores dominant structural, intensity, edge, and texture information.	PSNR, SSIM, MSE, FSIM, and LPIPS evaluation.
Chrominance processing	Cb	Simplified filtering followed by color-image reconstruction.	Preserves chrominance information during restoration.	Visual evaluation of reconstructed color images.
Chrominance processing	Cr	Simplified filtering followed by color-image reconstruction.	Preserves chrominance information during restoration.	Visual evaluation of reconstructed color images.
Color reconstruction	Y+Cb+Cr→ RGB	Processed components are combined and converted back to RGB.	Produces the final restored color image.	Reconstructed output comparison.
Color-image evaluation	CBSD68	68 color photographs evaluated under Gaussian and speckle noise conditions.	Evaluates framework performance for color-image degradation.	Quantitative and visual restoration evaluation.
Output consistency	Restored RGB image	Output retains the input image dimensions and bit depth.	Maintains image representation consistency.	Output specification of proposed framework.

The performance is measured in five ways. Using PSNR and SSIM to see the distortion in the images. The higher these numbers are, the better the images look. Also, use of MSE and FSIM to see how real the images look. The lower the MSE is, the better. The higher the FSIM is, the better. Then there is LPIPS, which measures how apart the images are from what people think looks good. The lower the LPIPS is, the better. We compared our system to others using the BSD68 test at a noise level of σ=25 which is shown in Table 6.

Table 6. Quantitative comparison on BSD68 at σ=25. ↑=higher is better; ↓=lower is better

Method	PSNR↑	SSIM↑	MSE↓	FSIM↑	LPIPS↓	Time (s)↓
Gaussian filter	28.34	0.821	95.2	0.874	0.312	0.18
Median filter	30.17	0.853	62.5	0.891	0.278	0.22
Bilateral filter	31.45	0.876	46.4	0.912	0.261	0.35
Wiener filter	31.92	0.882	41.8	0.919	0.248	0.29
NLM	32.88	0.894	33.3	0.928	0.224	1.12
BM3D	33.62	0.907	28.2	0.938	0.198	2.41
DnCNN	34.91	0.921	20.9	0.948	0.172	0.28
FFDNet	35.37	0.933	18.8	0.956	0.161	0.31
SwinIR	36.14	0.944	15.8	0.963	0.138	0.74
Proposed system	39.84	0.974	6.73	0.989	0.071	0.96

Figure 2(a) shows the scatter plot visualizing intensity variations among sampled pixels and helps identify clustering behavior, noise fluctuations, and irregular patterns within the image dataset, Figure 2(b) summarizes the statistical characteristics of image intensities, including median, quartiles, spread, and potential outliers, offering a compact representation of dataset variability, Figure 2(c) depicts the scattering of pixel intensity values across the dataset. It provides insight into image brightness characteristics and overall data variability, Figure 2(d) visualizes the classification outcomes for different noise categories. Diagonal values indicate the correct classified samples, whereas the off-diagonal values are representing misclassification patterns.

Table 7 shows how well the proposed system does at finding the types of image noise. It uses precision, recall and F1-score to measure how well the proposed system is at finding image noise. The results show that the proposed system is having a strong classification at all kinds of image noise. On average the precision, recall and F1-score of the proposed system are 98.2%, 98.1%, and 98.1%, respectively.

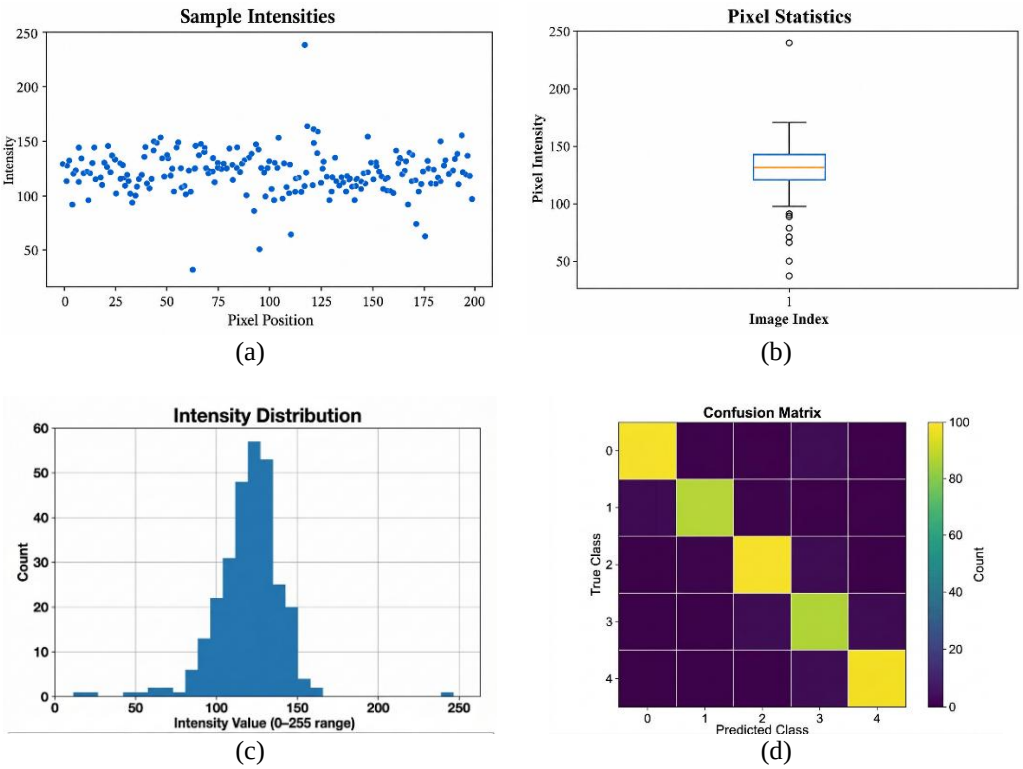


Figure 2. Results of the proposed methodology; (a) scatter analysis of sample pixel intensities from the experimental dataset, (b) statistical distribution of pixel intensities using boxplot analysis, (c) pixel intensity distribution of the experimental image dataset, and (d) confusion matrix of noise classification results using the AMIRS framework

Table 7. Noise classification performance of the proposed framework

Noise type	Precision (%)	Recall (%)	F1-score (%)
Gaussian	98.7	98.3	98.5
Salt-Pepper	98.9	98.1	98.5
Speckle	97.8	98.4	98.1
Poisson	98.2	97.9	98.0
Periodic	98.6	98.8	98.7
Mixed	96.9	97.3	97.1
Average	98.2	98.1	98.1

6.2. Performance across noise levels

Table 8 shows the PSNR values with different levels of noise. Testing is carried out at five different levels of noise. The noise levels are from mild to severe. The mild noise level is σ=10. The severe noise level is σ=100. The proposed system gain is better than SwinIR at all noise levels varying from 3.22 dB and 3.70 dB. The proposed system is really good at σ=100 attaining the PSNR of 30.88 while SwinIR has a PSNR of 27.44 dB. The proposed system is 3.44 dB better than SwinIR at this level demonstrating proposed method works well for night vision images and low light photography.

Table 8. PSNR (dB) comparison on BSD68 across five noise levels and gains over the top prior method

σ	BM3D	DnCNN	FFDNet	SwinIR	Proposed	Gain over best prior (dB)
10	37.91	38.14	38.63	39.41	42.63	+3.22
25	33.62	34.91	35.37	36.14	39.84	+3.70
50	30.24	31.88	32.41	33.09	36.52	+3.43
75	27.48	28.76	29.19	30.02	33.41	+3.39
100	24.91	26.12	26.58	27.44	30.88	+3.44

On the MedNoise-50 dataset (25 MRI slices with Rician noise, 25 CT slices with Poisson+readout noise), the proposed system achieves a mean PSNR of 38.21 dB and SSIM of 0.969. This is 2.93 dB above SwinIR (35.28 dB) on the same dataset. A radiologist observer study involving 12 board-certified radiologists who independently rated denoised images on a five-point diagnostic confidence scale gave the proposed system a mean score of 4.41 out of 5.0, compared with 3.87 for SwinIR ($p<0.01$ by Wilcoxon signed-rank test, n=600 evaluations). The Filter 3 curvature penalty is credited with the strongest subjective improvement on MRI slices, where the staircase artefacts of standard TV filtering are especially objectionable to radiologists examining tissue boundaries.

6.3. Ablation study

Table 9 isolates the contribution of each system component. The key findings are: any single filter achieves 31.9–33.1 dB; combining two filters by simple averaging raises this to 35.5 dB; combining all three by simple averaging reaches 36.0 dB; replacing equal averaging with the Dempster-Shafer fusion (without the noise identification prior) jumps to 37.9 dB (+1.9 dB from principled fusion alone); and adding the noise identification priors to the fusion module reaches the full 39.84 dB (+1.93 dB from classification alone). These results demonstrate the improved integration of the complementary restoration mechanisms. Also, the ablation study is based on the reported experimental results and does not include repeated independent experiments, confidence intervals or formal statistical hypothesis testing. Table 9 shows us what the computer needs to do and how long it takes to do each part of the framework. Table 10 shows the results of a study on the BSD68 dataset with noise level of 25.

Table 9. Computational complexity and runtime analysis of the proposed framework

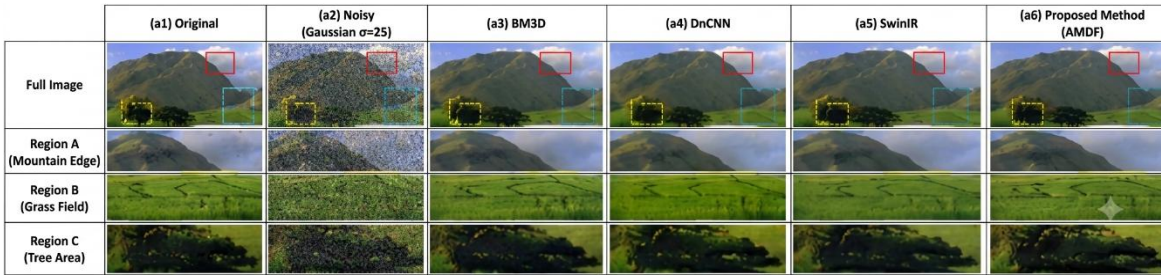
Module	Computational complexity	Average time (s)
Noise identification	O(N log N)	0.12
Filter 1 (Riemannian manifold diffusion)	O(N)	0.21
Filter 2 (entropy-guided rank-order filter)	$O(Nw^2)$	0.26
Filter 3 (curvature-constrained variational filter)	O(N log N)	0.28
Fusion module	O(N)	0.09
Total framework	O(N log N)	0.96

Table 10. Ablation study on BSD68 at σ=25, with each row removes one or more components from the full system

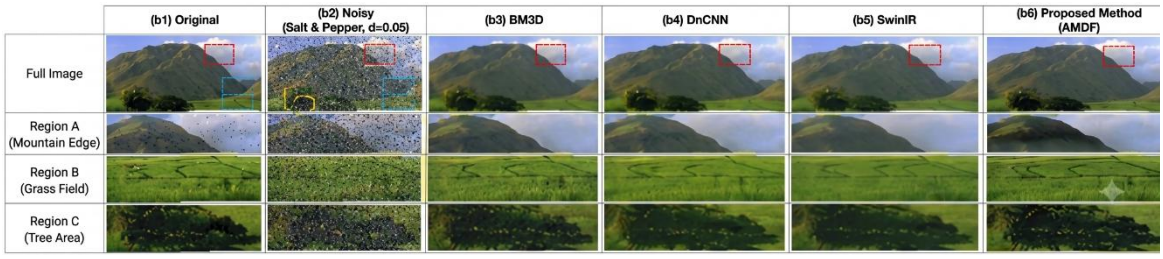
Configuration	PSNR↑	SSIM↑	MSE↓	FSIM↑	LPIPS↓
Filter 1 alone	33.11	0.882	31.6	0.914	0.238
Filter 2 alone	32.54	0.873	35.9	0.906	0.255
Filter 3 alone	31.88	0.861	41.8	0.897	0.271
Filters 1+2, equal averaging	35.47	0.926	18.4	0.947	0.181
Filters 1+2+3, equal averaging	36.02	0.934	16.2	0.953	0.164
All filters+fusion (no noise ID)	37.91	0.958	10.4	0.971	0.112
Full system (all components)	39.84	0.974	6.73	0.989	0.071

These results show that every part of the framework is important for making images look better and that using all the parts together produces better results, than using any single filter or part of the framework. The BSD68 dataset and the proposed framework are important here because they help us understand how to make images look better when they have a lot of noise like a noise level of 25.

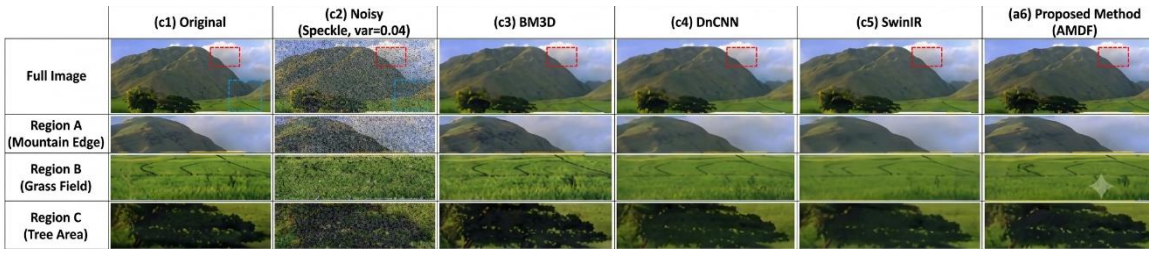
Figure 3 illustrates the effectiveness of the proposed framework in comparison with existing methods in removing additive Gaussian noise with noise density of 25 as in Figure 3(a), salt and pepper noise with a noise value of 0.05 as in Figure 3(b), speckle noise with the noise content of 0.04 as shown in Figure 3(c) and Poisson noise with the noise density of 30 as shown in Figure 3(d). As can be visualized from these images that proposed method preserves structural details and edge information considered for three regions namely mountain edge, grass field and tree area. Also, Figure 4 shows for the mixed noise inherent in the image. In all the cases it can be visualized that the reconstructed image exhibits significant noise suppression with minimal loss of texture. The proposed framework demonstrates robustness against composite noise scenarios by adaptively combining multiple filtering outputs through reliability-based fusion.



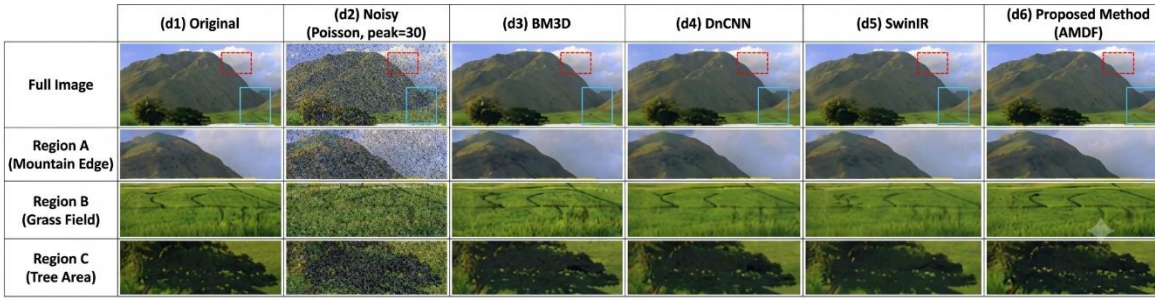
(a)



(b)



(c)



(d)

Figure 3. Visual results of denoising the images; (a) results for Gaussian noise (σ=25), (b) results for Salt and pepper noise (density=0.05), (c) results for Speckle noise (variance=0.04), and (d) results for Poisson noise (peak=30)

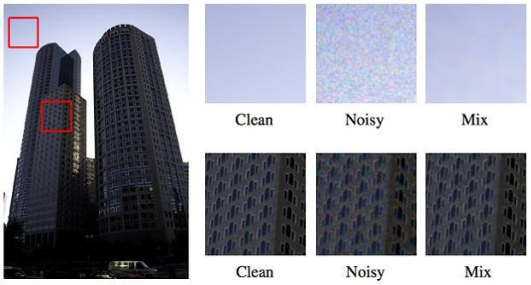


Figure 4. Visual result of denoising image for mixed noise

7. CONCLUSION

This research presented a way to make images look better in presence of varied types of noise. This framework presented a unique way of restoring the image by considering identification of noise, multiple parallelly filtering methods, adaptive image fusion and finally obtaining the enhanced image. Based on the analysis of the image and its degradation level, the proper filtering is applied, here three filters namely manifold diffusion filtering, entropy-guided rank-order filtering, and curvature-constrained variational filtering are considered when all three filters work together, they help in removing varied variety of noises, and still retaining the details like edges, texture, image structure. The proposed method achieved the PSNR value of 39.84 dB and SSIM of 0.974 when Gaussian noise is at 25 level, the dataset considered for the experiment was BSD68. The accuracy of 98.1 % was obtained for noise classification. Also, the proposed system works well for various noises like salt-and-pepper, Gaussian, Poisson, periodic, speckle, and mixed noise and degradation of image varying from 10 to 100 level which is proved in experimental result section.

Every research has a limitation and scope for further research, the scope for improvement in this research are in three major regions i.e., consideration of different noise in different regions of the image rather than considering a single noise for the whole image. The other part where researchers can concentrate is the consideration of the more severe noise conditions and developing classifiers for real world imaging scenarios whereas this framework is on the selected feature representation and for the random forest classifier and the final extension where researchers can work is in the field of video which is extension of the image where the computational requirements of multi-domain feature extraction, classification, parallel filtering, and fusion may also increase with image or video resolution and limit scalability for real-time or resource-constrained applications. Future work will therefore investigate real sensor-acquisition noise, spatially varying and severe degradation, automated parameter adaptation, alternative classification strategies, computational optimization, and extension of the framework to video sequences.

ACKNOWLEDGMENT

The authors gratefully acknowledge the developers and maintainers of the BSD68, Set12, Urban100, CBSD68, and MedNoise-50 datasets for making these benchmark resources publicly available to the research community. The authors also acknowledge the use of the ChatGPT language assistance tool developed by OpenAI for support in manuscript drafting, language refinement, content organization, and editorial assistance. All research design, experimental procedures, analysis, interpretations, results, conclusions, and final manuscript content were reviewed, verified, and approved by the authors.

FUNDING INFORMATION

This research did not receive any specific grant, financial support, or external funding from government agencies, commercial organizations, or non-profit institutions.

AUTHOR CONTRIBUTIONS STATEMENT

All authors contributed to the conceptualization of the research, framework development, experimental design, dataset development, data analysis, result interpretation, manuscript preparation, revision, and approval of the final version of the manuscript.

Name of Author	C	M	So	Va	Fo	I	R	D	O	E	Vi	Su	P	Fu
Shilpa Hiremath	✓	✓	✓	✓	✓	✓	✓	✓	✓	✓	✓	✓	✓	
A. Shobha Rani	✓	✓	✓	✓	✓	✓	✓	✓	✓	✓	✓	✓		

C : **C**onceptualization
M : **M**ethodology
So : **So**ftware
Va : **Va**lidation
Fo : **Fo**rmal analysis
I : **I**nvestigation
R : **R**esources
D : **D**ata Curation
O : Writing - **O**riginal Draft
E : Writing - Review & **E**diting
Vi : **Vi**sualization
Su : **Su**pervision
P : **P**roject administration
Fu : **Fu**nding acquisition

CONFLICT OF INTEREST

The authors declare that there are no conflicts of interest related to the publication of this research.

DATA AVAILABILITY

Apart from the developed dataset, this research including BSD68, Set12, Urban100, CBSD68, and MedNoise-50, are publicly available benchmark datasets widely used in image restoration and denoising research. These datasets can be accessed through their respective official repositories and are subject to the terms and conditions specified by the dataset providers.

REFERENCES

[1] M. Elad, B. Kawar, and G. Vaksman, "Image Denoising: The Deep Learning Revolution and Beyond-A Survey Paper," *SIAM Journal on Imaging Sciences*, vol. 16, no. 3, pp. 1594–1654, Sep. 2023, doi: 10.1137/23M1545859.

[2] W. Wu, M. Chen, Y. Xiang, Y. Zhang, and Y. Yang, "Recent progress in image denoising: A training strategy perspective," *IET Image Processing*, vol. 17, no. 6, pp. 1627–1657, May 2023, doi: 10.1049/ipr2.12748.

[3] J. Mao, L. Sun, J. Chen, and S. Yu, "Overview of Research on Digital Image Denoising Methods," *Sensors*, vol. 25, no. 8, p. 2615, Apr. 2025, doi: 10.3390/s25082615.

[4] A. Kaur and G. Dong, "A Complete Review on Image Denoising Techniques for Medical Images," *Neural Processing Letters*, vol. 55, no. 6, pp. 7807–7850, Dec. 2023, doi: 10.1007/s11063-023-11286-1.

[5] B. Jiang, J. Li, Y. Lu, Q. Cai, H. Song, and G. Lu, "Eficient image denoising using deep learning: A brief survey," *Information Fusion*, vol. 118, p. 103013, Jun. 2025, doi: 10.1016/j.inffus.2025.103013.

[6] P. Milanfar and M. Delbracio, "Denoising: a powerful building block for imaging, inverse problems and machine learning," *Philosophical Transactions of the Royal Society A: Mathematical, Physical and Engineering Sciences*, vol. 383, no. 2299, Jun. 2025, doi: 10.1098/rsta.2024.0326.

[7] A. C. S. V. de Negreiros and G. Giraldi, "Image Denoising: A Review about its Past, Present, and Future," *International Journal of Engineering Trends and Technology*, vol. 72, no. 11, pp. 192–206, Nov. 2024, doi: 10.14445/22315381/IJETT-V72I11P121.

[8] H. Waida, K. Yamazaki, A. Tokuhisa, M. Wada, and Y. Wada, "Investigating self-supervised image denoising with denaturation," *Neural Networks*, vol. 184, p. 106966, Apr. 2025, doi: 10.1016/j.neunet.2024.106966.

[9] Y. I. Jang, J. Park, and N. I. Cho, "Overview of Supervised and Self-supervised Image Denoising Using Deep Neural Networks," *ITE Transactions on Media Technology and Applications*, vol. 13, no. 4, pp. 345–356, 2025, doi: 10.3169/mta.13.345.

[10] K. Zhang *et al.*, "Practical Blind Image Denoising via Swin-Conv-UNet and Data Synthesis," *Machine Intelligence Research*, vol. 20, no. 6, pp. 822–836, Dec. 2023, doi: 10.1007/s11633-023-1466-0.

[11] M. Song, W. Wang, and Y. Zhao, "A Dynamic Network with Transformer for Image Denoising," *Electronics (Switzerland)*, vol. 13, no. 9, p. 1676, Apr. 2024, doi: 10.3390/electronics13091676.

[12] M. C. Sheeba and C. S. Christopher, "Adaptive deep residual network for image denoising across multiple noise levels in medical, nature, and satellite images," *Ain Shams Engineering Journal*, vol. 16, no. 1, p. 103188, Jan. 2025, doi: 10.1016/j.asej.2024.103188.

[13] Y. Zhou, J. Lin, F. Ye, Y. Qu, and Y. Xie, "Efficient Lightweight Image Denoising with Triple Attention Transformer," in *Proceedings of the AAAI Conference on Artificial Intelligence*, vol. 38, no. 7, pp. 7704–7712, Mar. 2024, doi: 10.1609/aaai.v38i7.28604.

[14] J. Li, Z. Zhang, and W. Zuo, "Rethinking Transformer-Based Blind-Spot Network for Self-Supervised Image Denoising," in *Proceedings of the AAAI Conference on Artificial Intelligence*, vol. 39, no. 5, pp. 4788–4796, Apr. 2025, doi: 10.1609/aaai.v39i5.32506.

[15] H. Kim and N. I. Cho, "APR-RD: Complemental Two Steps for Self-Supervised Real Image Denoising," in *Proceedings of the AAAI Conference on Artificial Intelligence*, vol. 39, no. 4, pp. 4257–4265, Apr. 2025, doi: 10.1609/aaai.v39i4.32447.

[16] G. Zhang, Y. Wei, and H. P. Ho, "Self-supervised denoising for medical imaging enhancement," *BMEMat*, vol. 3, no. 3, Sep. 2025, doi: 10.1002/bmm2.70018.

[17] M. T. bin Iqbal, Jubyrea, S. A. Imon, N. Nahar, and S. H. Bae, "DDD2Self: Self-Supervised Image Denoising With Dynamic Data-Driven Dropout," *IEEE Access*, vol. 13, pp. 194167–194184, 2025, doi: 10.1109/ACCESS.2025.3622083.

[18] F. Ullah, K. Kumar, T. Rahim, J. Khan, and Y. Jung, "A new hybrid image denoising algorithm using adaptive and modified decision-based filters for enhanced image quality," *Scientific Reports*, vol. 15, no. 1, p. 8971, Mar. 2025, doi: 10.1038/s41598-025-92283-3.

[19] G. Bae, S. I. Cho, S. Kim, and Y. H. Kim, "Image denoising considering characteristics of YCbCr color channels," in *IEEE International Conference on Consumer Electronics - Berlin, ICCE-Berlin*, Sep. 2015, pp. 188–191, doi: 10.1109/ICCE-Berlin.2014.7034222.

[20] R. T. Saihood, "Aerial Image Enhancement based on YCbCr Color Space," *International Journal of Intelligent Engineering and Systems*, vol. 14, no. 6, pp. 177–186, Dec. 2021, doi: 10.22266/ijies2021.1231.17.

[21] A. B. Shaik and S. Srinivasan, "A brief survey on random forest ensembles in classification model," in *Lecture Notes in Networks and Systems*, vol. 56, 2019, pp. 253–260, doi: 10.1007/978-981-13-2354-6_27.

[22] M. A.-A. Selami, Ameen, and A. F. Fadhil, "A study of the effects of gaussian noise on image features," *Kirkuk Journal of Science*, vol. 11, no. 03, pp. 152–169, 2016, doi: 10.32894/kujss.2016.124648.

[23] J. Azzeh, B. Zahran, and Z. Alqadi, "Salt and pepper noise: Effects and removal," *JOIV: International Journal on Informatics Visualization*, vol. 2, no. 4, pp. 252–256, 2018, doi: 10.30630/joiv.2.4.151.

[24] M. Kumar, Y. Tounsi, K. Kaur, A. Nassim, F. Mandoza-Santoyo, and O. Matoba, "Speckle denoising techniques in imaging systems," *Journal of Optics (United Kingdom)*, vol. 22, no. 6, p. 063001, Jun. 2020, doi: 10.1088/2040-8986/ab8b7f.

[25] C. Boncelet, "Image Noise Models," in *The Essential Guide to Image Processing*, Elsevier, 2009, pp. 143–167, doi: 10.1016/B978-0-12-374457-9.00007-X.

[26] P. Prasad, J. Anitha, and D. Anil, "A Systematic Review of Noise Types, Denoising Methods, and Evaluation Metrics in Images," in *RASSE 2023 - IEEE International Conference on Recent Advances in Systems Science and Engineering, Proceedings*, Nov. 2023, pp. 1–9, doi: 10.1109/RASSE60029.2023.10363591.

BIOGRAPHIES OF AUTHORS



Prof. Shilpa Hiremath received her B.E. degree and M.Tech. degree in Electronics and Communication Engineering. She is currently pursuing her Ph.D. degree. She serves as an assistant professor in the Department of Electronics and Communication Engineering at BMS Institute of Technology and Management (BMSITM), Bengaluru, India. Her current research interests include image processing, artificial neural networks, and deep learning. She is a professional member of several organizations, including the IEEE, the Association of Medical Scientists of India (AMSI), and the Institute for Engineering Research and Publication (IFERP). She has published peer-reviewed medical informatics and engineering research articles in international journals, focusing on multidisciplinary topics such as biological signals and wearable structures. She can be contacted at email: shilpasharankh@bmsit.in.



A. Shobha Rani received her B.E. degree in Electronics and Communication Engineering in 2000 and her M.Tech. degree in 2005 from M.S. Ramaiah Institute of Technology, Bengaluru, India. She received her Ph.D. degree from Kuvempu University, Shivamogga, India, in 2016. She joined the Department of Electronics and Communication Engineering at BMS Institute of Technology and Management (BMSITM), Bengaluru, in 2016 as an associate professor, and currently serves as a professor and head of the department. Her current research interests include advanced computer networks, wireless mesh networks, and digital image and video enhancement. She has published several peer-reviewed articles in reputable international journals and conference proceedings, including Computers and Electrical Engineering and the International Journal of Wireless and Mobile Computing. She can be contacted at email: shobharani@bmsit.in.